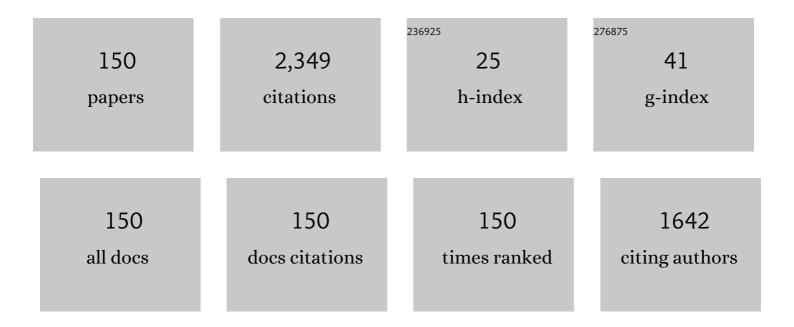
## List of Publications by Year in descending order

Source: https://exaly.com/author-pdf/3575223/publications.pdf Version: 2024-02-01



#	Article	IF	CITATIONS
1	Lidar Ratio Regional Transfer Method for Extinction Coefficient Accuracy Improvement in Lidar Networks. Remote Sensing, 2022, 14, 626.	4.0	0
2	Water Cloud Detection with Circular Polarization Lidar: A Semianalytic Monte Carlo Simulation Approach. Sensors, 2022, 22, 1679.	3.8	2
3	Detection of surface defects and subsurface defects of polished optics with multisensor image fusion. PhotoniX, 2022, 3, .	13.5	26
4	Dual-field-of-view high-spectral-resolution lidar: Simultaneous profiling of aerosol and water cloud to study aerosol–cloud interaction. Proceedings of the National Academy of Sciences of the United States of America, 2022, 119, e2110756119.	7.1	15
5	Embedded laser frequency locking for HSRL applications with an iodine absorption cell. , 2022, , .		0
6	LiDAR Remote Sensing for Vertical Distribution of Seawater Optical Properties and Chlorophyll-a From the East China Sea to the South China Sea. IEEE Transactions on Geoscience and Remote Sensing, 2022, 60, 1-21.	6.3	4
7	Real-time detection method for bulk bubbles in optics based on deep learning. Applied Optics, 2022, 61, 4344.	1.8	0
8	Multiple scattering effect of water clouds on spaceborne oceanic lidar signals. Journal of Quantitative Spectroscopy and Radiative Transfer, 2022, 288, 108253.	2.3	0
9	Confocal laser scanning and 3D reconstruction methods for the subsurface damage of polished optics. Optics and Lasers in Engineering, 2021, 136, 106315.	3.8	14
10	Compact, snapshot and triple-wavelength system for ICF target ice-layer refractive index and thickness measurement. Optics and Laser Technology, 2021, 134, 106595.	4.6	3
11	Automatic evaluation system for bulk defects in optics. Optics and Lasers in Engineering, 2021, 137, 106380.	3.8	8
12	Non-null interferometers for irregular surface measurement with system modeling. Measurement Science and Technology, 2021, 32, 045205.	2.6	0
13	Development of ZJU high-spectral-resolution lidar for aerosol and cloud: Feature detection and classification. Journal of Quantitative Spectroscopy and Radiative Transfer, 2021, 261, 107513.	2.3	13
14	Compact wavelength tunable output around 440 nm pulsed laser for oceanic lidar application. Optics Communications, 2021, 485, 126706.	2.1	5
15	Optical system design for a hyperspectral imaging lidar using supercontinuum laser and its preliminary performance. Optics Express, 2021, 29, 17542.	3.4	9
16	Refractive index distribution of the ice-layer in ICF target from the interference method. Optics and Laser Technology, 2021, 138, 106860.	4.6	1
17	Vertical distribution of subsurface phytoplankton layer in South China Sea using airborne lidar. Remote Sensing of Environment, 2021, 263, 112567.	11.0	29
18	Retrieval of aerosol liquid water content from high spectral resolution lidar. Science of the Total Environment, 2021, 799, 149423.	8.0	4

#	Article	IF	CITATIONS
19	Study on Single-Terminal Transmission Visibility Meter based on reflector. , 2021, , .		0
20	Absolute measurement approach for crystal growth height based on a polarization-synchronized phase-shifting interferometer. Applied Optics, 2021, 60, 9721.	1.8	1
21	Phase unwrapping in ICF target interferometric measurement via deep learning. Applied Optics, 2021, 60, 10.	1.8	8
22	Interferometric measurement of freeform surfaces using irregular subaperture stitching. Measurement Science and Technology, 2020, 31, 055202.	2.6	6
23	Detection of Chlorophyll a and CDOM Absorption Coefficient with a Dual-Wavelength Oceanic Lidar: Wavelength Optimization Method. Remote Sensing, 2020, 12, 3021.	4.0	5
24	Optimum wavelength of spaceborne oceanic lidar in penetration depth. Journal of Quantitative Spectroscopy and Radiative Transfer, 2020, 256, 107310.	2.3	9
25	Oceanic Lidar: Theory and Experiment. EPJ Web of Conferences, 2020, 237, 07021.	0.3	1
26	Determination of Planetary Boundary Layer height with Lidar Signals Using Maximum Limited Height Initialization and Range Restriction (MLHI-RR). Remote Sensing, 2020, 12, 2272.	4.0	15
27	3D Transparent Object Detection and Reconstruction Based on Passive Mode Single-Pixel Imaging. Sensors, 2020, 20, 4211.	3.8	8
28	Retrieval of Aerosol Optical Properties Based on High Spectral Resolution Lidar. EPJ Web of Conferences, 2020, 237, 08018.	0.3	0
29	Performance Evaluation of Spaceborne Integrated Path Differential Absorption Lidar for Carbon Dioxide Detection at 1572 nm. Remote Sensing, 2020, 12, 2570.	4.0	6
30	A Semianalytic Monte Carlo Simulator for Spaceborne Oceanic Lidar: Framework and Preliminary Results. Remote Sensing, 2020, 12, 2820.	4.0	11
31	Development of ZJU high-spectral-resolution lidar for aerosol and cloud: Calibration of overlap function. Journal of Quantitative Spectroscopy and Radiative Transfer, 2020, 257, 107338.	2.3	11
32	Development of ZJU High-Spectral-Resolution Lidar for Aerosol and Cloud: Extinction Retrieval. Remote Sensing, 2020, 12, 3047.	4.0	12
33	Construction of Nighttime Cloud Layer Height and Classification of Cloud Types. Remote Sensing, 2020, 12, 668.	4.0	7
34	Design and validation of a shipborne multiple-field-of-view lidar for upper ocean remote sensing. Journal of Quantitative Spectroscopy and Radiative Transfer, 2020, 254, 107201.	2.3	10
35	Retrievals of aerosol layer height during dust events over the taklimakan and gobi desert. Journal of Quantitative Spectroscopy and Radiative Transfer, 2020, 254, 107198.	2.3	5
36	Optimization of the OCO-2 Cloud Screening Algorithm and Evaluation against MODIS and TCCON Measurements over Land Surfaces in Europe and Japan. Advances in Atmospheric Sciences, 2020, 37, 387-398.	4.3	1

#	Article	IF	CITATIONS
37	Instrument response effects on the retrieval of oceanic lidar. Applied Optics, 2020, 59, C21.	1.8	7
38	Detailed investigation of the iterative analysis for inertial confinement fusion target characterization. Applied Optics, 2020, 59, 10880.	1.8	1
39	Lidar Remote Sensing of Seawater Optical Properties: Experiment and Monte Carlo Simulation. IEEE Transactions on Geoscience and Remote Sensing, 2019, 57, 9489-9498.	6.3	33
40	Random two-frame phase-shifting interferometry via minimization of coefficient of variation. Applied Physics Letters, 2019, 115, .	3.3	13
41	Validation of the Analytical Model of Oceanic Lidar Returns: Comparisons with Monte Carlo Simulations and Experimental Results. Remote Sensing, 2019, 11, 1870.	4.0	19
42	A semianalytic Monte Carlo radiative transfer model for polarized oceanic lidar: Experiment-based comparisons and multiple scattering effects analyses. Journal of Quantitative Spectroscopy and Radiative Transfer, 2019, 237, 106638.	2.3	21
43	Program of Spaceborne Oceanic Lidar Based on Semianalytic Monte Carlo Method. , 2019, , .		0
44	Analysis of global three-dimensional aerosol structure with spectral radiance matching. Atmospheric Measurement Techniques, 2019, 12, 6541-6556.	3.1	6
45	Comparing black and brown carbon absorption from AERONET and surface measurements at wintertime Fresno. Atmospheric Environment, 2019, 199, 164-176.	4.1	20
46	Misalignment correction for free-form surface in non-null interferometric testing. Optics Communications, 2019, 437, 204-213.	2.1	6
47	Design of a high-spectral-resolution lidar for atmospheric temperature measurement down to the near ground. Applied Optics, 2019, 58, 9651.	1.8	9
48	Backscattering ratios of soot-contaminated dusts at triple LiDAR wavelengths: T-matrix results. Optics Express, 2019, 27, A92.	3.4	20
49	Performance estimation of space-borne high-spectral-resolution lidar for cloud and aerosol optical properties at 532 nm. Optics Express, 2019, 27, A481.	3.4	19
50	Phase function effects on the retrieval of oceanic high-spectral-resolution lidar. Optics Express, 2019, 27, A654.	3.4	14
51	Retrieving the microphysical properties of opaque liquid water clouds from CALIOP measurements. Optics Express, 2019, 27, 34126.	3.4	5
52	Universal phase reconstruction approach of self-calibrating phase-shifting interferometry. Optics Letters, 2019, 44, 3857.	3.3	9
53	Multiple scattering effects on the return spectrum of oceanic high-spectral-resolution lidar. Optics Express, 2019, 27, 30204.	3.4	4
54	Real-time pedestrian crossing lights detection algorithm for the visually impaired. Multimedia Tools and Applications, 2018, 77, 20651-20671.	3.9	26

#	Article	IF	CITATIONS
55	100 MW Peak Power Picosecond Laser Based on Hybrid End-Pumped Nd:YVO4 and Side-Pumped Nd:YAG Amplifiers. IEEE Journal of Selected Topics in Quantum Electronics, 2018, 24, 1-7.	2.9	12
56	Rotating a half-wave plate by 45°: An ideal calibration method for the gain ratio in polarization lidars. Optics Communications, 2018, 407, 361-366.	2.1	5
57	Assessing the depolarization capabilities of nonspherical particles in a super-ellipsoidal shape space. Optics Express, 2018, 26, 1726.	3.4	57
58	ICF target DT-layer refractive index and thickness from iterative analysis. Optics Express, 2018, 26, 17781.	3.4	6
59	Effects of auxiliary atmospheric state parameters on the aerosol optical properties retrieval errors of high-spectral-resolution lidar. Applied Optics, 2018, 57, 2627.	1.8	10
60	Fast and accurate wavefront reconstruction in two-frame phase-shifting interferometry with unknown phase step. Optics Letters, 2018, 43, 3033.	3.3	22
61	Relationship between the effective attenuation coefficient of spaceborne lidar signal and the IOPs of seawater. Optics Express, 2018, 26, 30278.	3.4	19
62	A pressure-tuned field-widened Michelson interferometer system as the spectroscopic filter of high-spectral-resolution lidar. , 2018, , .		0
63	Determination of thermally induced effects and design guidelines of optomechanical accelerometers. Measurement Science and Technology, 2017, 28, 115201.	2.6	5
64	Practical retrace error correction in non-null aspheric testing: A comparison. Optics Communications, 2017, 383, 378-385.	2.1	17
65	Polarization properties of receiving telescopes in atmospheric remote sensing polarization lidars. Applied Optics, 2017, 56, 6837.	1.8	12
66	Design of iodine absorption cell for high-spectral-resolution lidar. Optics Express, 2017, 25, 15913.	3.4	27
67	Generalized high-spectral-resolution lidar technique with a multimode laser for aerosol remote sensing. Optics Express, 2017, 25, 979.	3.4	10
68	Retrieving the seawater volume scattering function at the 180° scattering angle with a high-spectral-resolution lidar. Optics Express, 2017, 25, 11813.	3.4	15
69	Use of Debye's series to determine the optimal edge-effect terms for computing the extinction efficiencies of spheroids. Optics Express, 2017, 25, 20298.	3.4	13
70	Aerosol Optical Properties over China from RAMS-CMAQ Model Compared with CALIOP Observations. Atmosphere, 2017, 8, 201.	2.3	7
71	Testing of an off-axis parabolic mirror based on hybrid compensation technology. , 2017, , .		0
72	Effects of a nonideal half-wave plate on the gain ratio calibration measurements in polarization lidars. Applied Optics, 2017, 56, 8100.	1.8	1

#	Article	IF	CITATIONS
73	Design of the interferometric spectral discrimination filters for a three-wavelength high-spectral-resolution lidar. Optics Express, 2016, 24, 27622.	3.4	5
74	Numerical simulation research and applications on scattering imaging of surface defects on optical components. , 2016, , .		3
75	High-spectral-resolution lidar for ocean biological carbon pump studies. , 2016, , .		1
76	Field-widened Michelson interferometer for spectral discrimination in high-spectral-resolution lidar: practical development. Optics Express, 2016, 24, 7232.	3.4	13
77	Polarized high-spectral-resolution lidar based on field-widened Michelson interferometer. Proceedings of SPIE, 2016, , .	0.8	1
78	Comprehensive view of high-spectral-resolution lidar technique from the perspective of spectral discrimination. Proceedings of SPIE, 2016, , .	0.8	0
79	Defects evaluation system for spherical optical surfaces based on microscopic scattering dark-field imaging method. Applied Optics, 2016, 55, 6162.	2.1	38
80	Beam quality management by periodic reproduction of wavefront aberrations in end-pumped Nd:YVO_4 laser amplifiers. Optics Express, 2016, 24, 8988.	3.4	8
81	Frequency locking of a field-widened Michelson interferometer based on optimal multi-harmonics heterodyning. Optics Letters, 2016, 41, 3916.	3.3	7
82	Aspheric and free-form surfaces test with non-null sub-aperture stitching. , 2016, , .		1
83	Error analysis of spherical scanning mechanism used for surface defects detection. Proceedings of SPIE, 2016, , .	0.8	0
84	Minimizing cross-axis sensitivity in grating-based optomechanical accelerometers. Optics Express, 2016, 24, 9094.	3.4	40
85	Field-widened Michelson interferometer system as the spectroscopic filter of high-spectral-resolution lidar. , 2016, , .		Ο
86	High-spectral-resolution lidar for ocean ecosystem studies. Proceedings of SPIE, 2016, , .	0.8	3
87	Research on auto-centering device in surface defects evaluation system of large spherical optics. Proceedings of SPIE, 2016, , .	0.8	Ο
88	Algorithms and applications of aberration correction and American standard-based digital evaluation in surface defects evaluating system. Proceedings of SPIE, 2016, , .	0.8	1
89	Practical phase unwrapping of interferometric fringes based on unscented Kalman filter technique. Optics Express, 2015, 23, 32337.	3.4	58
90	Gravitational wave astronomy: the current status. Science China: Physics, Mechanics and Astronomy, 2015, 58, 1.	5.1	26

#	Article	IF	CITATIONS
91	Non-null annular subaperture stitching interferometry for aspheric test. , 2015, , .		0
92	Model-based phase-shifting interferometer. , 2015, , .		0
93	Recent developments of interferometric wavefront sensing. , 2015, , .		0
94	Retrieval of high-spectral-resolution lidar for atmospheric aerosol optical properties profiling. Proceedings of SPIE, 2015, , .	0.8	0
95	Earth observation and atmospheric sounding based on a high spectral resolution lidar. Proceedings of SPIE, 2015, , .	0.8	0
96	General measurement of optical system aberrations with a continuously variable lateral shear ratio by a randomly encoded hybrid grating. Applied Optics, 2015, 54, 8913.	2.1	19
97	Precisely connected and calculated algorithm of punctate scratches in the super-smooth surface defects evaluation system. Proceedings of SPIE, 2015, , .	0.8	0
98	The next detectors for gravitational wave astronomy. Science China: Physics, Mechanics and Astronomy, 2015, 58, 1.	5.1	23
99	A high-resolution detecting system based on machine vision for defects on large aperture and super-smooth surface. , 2015, , .		1
100	Determination of aspheric vertex radius of curvature in non-null interferometry. Applied Optics, 2015, 54, 2838.	1.8	16
101	Pattern recognition model for aerosol classification with atmospheric backscatter lidars: principles and simulations. Journal of Applied Remote Sensing, 2015, 9, 096006.	1.3	12
102	Field-widened Michelson interferometer for spectral discrimination in high-spectral-resolution lidar: theoretical framework. Optics Express, 2015, 23, 12117.	3.4	27
103	Aspheric subaperture stitching based on system modeling. Optics Express, 2015, 23, 19176.	3.4	28
104	Compact wavefront diagnosis system based on the randomly encoded hybrid grating. Proceedings of SPIE, 2015, , .	0.8	1
105	Retrieval of phase distributions from the quadriwave lateral shearing interferogram obtained by randomly encoded hybrid grating. , 2015, , .		5
106	Reverse optimization reconstruction method in non-null aspheric interferometry. Proceedings of SPIE, 2015, , .	0.8	0
107	Quadriwave lateral shearing interferometer based on a randomly encoded hybrid grating. Optics Letters, 2015, 40, 2245.	3.3	40
108	Aberration calibration in high-NA spherical surfaces measurement on point diffraction interferometry. Applied Optics, 2015, 54, 3877.	2.1	12

#	Article	IF	CITATIONS
109	Effects of spectral discrimination in high-spectral-resolution lidar on the retrieval errors for atmospheric aerosol optical properties. Applied Optics, 2014, 53, 4386.	1.8	29
110	Non-null annular subaperture stitching interferometry for steep aspheric measurement. Applied Optics, 2014, 53, 5755.	1.8	36
111	Reverse optimization reconstruction of aspheric figure error in a non-null interferometer. Applied Optics, 2014, 53, 5538.	1.8	36
112	Common-path and compact wavefront diagnosis system based on cross grating lateral shearing interferometer. Applied Optics, 2014, 53, 7144.	1.8	24
113	Grayscale adjustment method for CCD mosaic camera in surface defect detection system. Proceedings of SPIE, 2014, , .	0.8	1
114	Digital calibration method for defects evaluation of large fine optical surfaces. , 2014, , .		1
115	Automated discrimination between digs and dust particles on optical surfaces with dark-field scattering microscopy. Applied Optics, 2014, 53, 5131.	1.8	39
116	Distortion correction in surface defects evaluating system of large fine optics. Optics Communications, 2014, 312, 110-116.	2.1	21
117	Sparse microdefect evaluation system for large fine optical surfaces based on dark-field microscopic scattering imaging. , 2013, , .		8
118	Wavefront retrieval for cross-grating lateral shearing interferometer based on differential Zernike polynomial fitting. , 2013, , .		18
119	Off-axis cyclic radial shearing interferometer for measurement of centrally blocked transient wavefront. Optics Letters, 2013, 38, 2493.	3.3	17
120	Dark-field microscopic image stitching method for surface defects evaluation of large fine optics. Optics Express, 2013, 21, 5974.	3.4	68
121	Retrieval and analysis of a polarized high-spectral-resolution lidar for profiling aerosol optical properties. Optics Express, 2013, 21, 13084.	3.4	52
122	Interferometric filters for spectral discrimination in high-spectral-resolution lidar: performance comparisons between Fabry–Perot interferometer and field-widened Michelson interferometer. Applied Optics, 2013, 52, 7838.	1.8	21
123	Practical and accurate method for aspheric misalignment aberrations calibration in non-null interferometric testing. Applied Optics, 2013, 52, 8501.	1.8	31
124	Comparisons between field-widen Michelson interferometer and Fabry-Perot interferometer as the spectroscopic filter in high spectral resolution lidar. , 2013, , .		1
125	Design of a field-widened Michelson interferometer for a near-infrared high spectral resolution lidar. , 2013, , .		0
126	Mathematical modeling analysis on a small and compact two-dimensional CGLSI interference system. Proceedings of SPIE, 2013, , .	0.8	3

#	Article	IF	CITATIONS
127	A spectroscopic transmittance analytical modeling for field-widened Michelson interferometer employed by high spectral resolution lidars. Proceedings of SPIE, 2013, , .	0.8	3
128	Development of a field-widened Michelson spectroscopic filter for a polarized near-infrared high spectral resolution lidar. Proceedings of SPIE, 2013, , .	0.8	3
129	Development of the ZJU polarized near-infrared high spectral resolution lidar. Proceedings of SPIE, 2013, , .	0.8	0
130	System analysis of a tilted field-widened Michelson interferometer for high spectral resolution lidar. Optics Express, 2012, 20, 1406.	3.4	39
131	The Three-Dimensional Structure of Transatlantic African Dust Transport: A New Perspective from CALIPSO LIDAR Measurements. Advances in Meteorology, 2012, 2012, 1-9.	1.6	26
132	Tilted pressure-tuned field-widened Michelson interferometer for high spectral resolution lidar. Proceedings of SPIE, 2012, , .	0.8	4
133	Research on digital calibration method for optical surface defect dimension. Proceedings of SPIE, 2012, , .	0.8	2
134	Application of image entropy evaluation function for the leveling of large aperture components in auto defects detecting. Proceedings of SPIE, 2012, , .	0.8	1
135	Study on distortion correction for image mosaic of surface defects. , 2012, , .		1
136	High-precision technique for in-situ testing of the PZT scanner based on fringe analysis. Optics Communications, 2010, 283, 3115-3121.	2.1	9
137	Error analysis and system optimization of non-null aspheric testing system. , 2010, , .		1
138	Demodulation of a single complex fringe interferogram with a path-independent regularized phase-tracking technique. Applied Optics, 2010, 49, 170.	2.1	41
139	Research of precision interference locating method for a partial null compensator at aspheric testing. , 2009, , .		8
140	Non-null interferometric aspheric testing with partial null lens and reverse optimization. Proceedings of SPIE, 2009, , .	0.8	18
141	Practical methods for retrace error correction in nonnull aspheric testing. Optics Express, 2009, 17, 7025.	3.4	64
142	Climatology of drizzle in marine boundary layer clouds based on 1 year of data from CloudSat and Cloudâ€Aerosol Lidar and Infrared Pathfinder Satellite Observations (CALIPSO). Journal of Geophysical Research, 2008, 113, .	3.3	111
143	Global distribution of cirrus clouds from CloudSat/Cloudâ€Aerosol Lidar and Infrared Pathfinder Satellite Observations (CALIPSO) measurements. Journal of Geophysical Research, 2008, 113, .	3.3	365
144	Study on testing larger asphericity in non-null interferometer. Proceedings of SPIE, 2007, , .	0.8	7

#	Article	IF	CITATIONS
145	The position shifting of frequency spectrum of Fourier transform in the application of aspheric surface testing. , 2007, , .		0
146	The wavefront aberration analysis and testing accuracy evaluation for the large aberration aspheric system based on the best fit sphere. , 2007, , .		4
147	System optimization of radial shearing interferometer for aspheric testing. Proceedings of SPIE, 2007, ,	0.8	12
148	Real time diagnosis of transient pulse laser with high repetition by radial shearing interferometer. Applied Optics, 2007, 46, 8305.	2.1	40
149	Measurement of transient near-infrared laser pulse wavefront with high precision by radial shearing interferometer. Optics Communications, 2007, 275, 173-178.	2.1	18
150	Microscopic scattering imaging measurement and digital evaluation system of defects for fine optical surface. Optics Communications, 2007, 278, 240-246.	2.1	58